

Analysis of the polarization rotation effect in the inversely tapered spot size converter

Lianxi Jia,* Haifeng Zhou, Tsung-Yang Liow, Junfeng Song, Ying Huang, Xiaoguang Tu, Xianshu Luo, Chao Li, Qing Fang, Mingbin Yu, and Guoqiang Lo

*Institute of Microelectronics, A*STAR (Agency for Science, Technology and Research), 11 Science Park Road, Science Park II, 117685 Singapore*

**jialx@ime.a-star.edu.sg*

Abstract: Inversely tapered spot size converter (SSC) is widely used to connect silicon waveguide with fiber in silicon photonics. However, the tapered structure may cause polarization rotation and further generate interference fluctuation in the transmission spectrum even of a straight waveguide. We analyzed the light propagation in a straight waveguide with SSC at the both ends with coupling matrix and transmission matrix methods. The analysis results matched with the phenomena we observed in the transmission spectrum. Combining the analysis with the measurement results, we calculated the polarization rotation efficiency of the SSC in different samples and analyzed the origin of the polarization rotation effect. Finally, we discussed the influence of the effect to the DP-QPSK signal and proposed several methods to release the impact.

©2015 Optical Society of America

OCIS codes: (130.3120) Integrated optics devices; (230.7370) Waveguides; (060.4510) Optical communications.

References and links

1. T.-Y. Liow, J. F. Song, X. G. Tu, E.-J. Lim, Q. Fang, N. Duan, M. B. Yu, and G.-Q. Lo, "Silicon optical interconnect devices technologies for 40 Gb/s and Beyond," *IEEE J. Sel. Top. Quantum Electron.* **19**(2), 8200312 (2013).
2. V. R. Almeida, R. R. Panepucci, and M. Lipson, "Nanotaper for compact mode conversion," *Opt. Lett.* **28**(15), 1302–1304 (2003).
3. B. B. Bakir, A. V. de Gyves, R. Orobtcouk, P. Lyan, C. Porzier, A. Roman, and J.-M. Fedeli, "Low-loss (<1 dB) and polarization-insensitive edge fiber couplers fabricated on 200-mm silicon-on-insulator wafers," *IEEE Photonics Technol. Lett.* **22**(11), 739–741 (2010).
4. T. Shoji, T. Tsuchizawa, T. Watanabe, K. Yamada, and H. Morita, "Low loss mode size converter from 0.3 μm square Si wire waveguides to singlemode fibers," *Electron. Lett.* **38**(25), 1669–1670 (2002).
5. L. Chen, C. R. Doerr, Y.-K. Chen, and T.-Y. Liow, "Low-loss and broadband cantilever couplers between standard cleaved fibers and high-index-contrast Si₃N₄ or Si waveguides," *IEEE Photonics Technol. Lett.* **22**(23), 1744–1746 (2010).
6. Q. Fang, T. Y. Liow, J. F. Song, C. W. Tan, M. B. Yu, G. Q. Lo, and D. L. Kwong, "Suspended optical fiber-to-waveguide mode size converter for silicon photonics," *Opt. Express* **18**(8), 7763–7769 (2010).
7. L. Jia, J. Song, T.-Y. Liow, X. Luo, X. Tu, Q. Fang, S.-C. Koh, M. Yu, and G. Lo, "Mode size converter between high-index-contrast waveguide and cleaved single mode fiber using SiON as intermediate material," *Opt. Express* **22**(19), 23652–23660 (2014).
8. L. X. Jia, T.-Y. Liow, J. F. Song, X. S. Luo, N. Duan, S. C. Koh, Q. Fang, M. B. Yu, and G. Q. Lo, "Compact optical polarization rotators based on an asymmetric silicon waveguide," *IEEE Photonics Technol. Lett.* **25**(22), 2229–2232 (2013).
9. A. E.-J. Lim, T.-Y. Liow, J. F. Song, C. Li, Q. Fang, X. G. Tu, N. Duan, K. K. Chen, R. P. C. Tern, C. Peng, B. W. Mun, M. N. Islam, J. S. Park, C. Subbu, and G.-Q. Lo, "Path to silicon photonics commercialization: 25Gb/s platform development in a CMOS manufacturing foundry line," in *Optical Fiber Communication Conference*, paper Th2A.51 (2014).
10. Y. Vlasov and S. McNab, "Losses in single-mode silicon-on-insulator strip waveguides and bends," *Opt. Express* **12**(8), 1622–1631 (2004).
11. K. Goi, H. Kusaka, A. Oka, K. Ogawa, T.-Y. Liow, X. G. Tu, G.-Q. Lo, and D.-L. Kwong, "128-Gb/s DP-QPSK using low-loss monolithic silicon IQ modulator integrated with partial-rib polarization rotator," in *Optical Fiber Communication Conference*, paper W11.2 (2014).

12. P. Dong, X. Liu, S. Chandrasekhar, L. L. Buhl, R. Aroca, and Y.-K. Chen, "Monolithic silicon photonic integrated circuits for compact 100+Gb/s coherent optical receivers and transmitters," *IEEE J. Sel. Top. Quantum Electron.* **20**(4), 6100108 (2014).
13. M. Sjödin, P. Johannisson, P. A. Andrekson, and M. Karlsson, "Linear and nonlinear crosstalk tolerance of polarization-switched QPSK and polarization-multiplexed QPSK," in *European Conference on Optical Communication and Exhibition*, paper Mo.2.B.5 (2011).
14. S. J. Savory, "Digital coherent optical receivers: algorithms and subsystems," *IEEE J. Sel. Top. Quantum Electron.* **16**(5), 1164–1179 (2010).
15. Y. Huang, S. Y. Zhu, H. J. Zhang, T.-Y. Liow, and G. Q. Lo, "Ultra-compact CMOS compatible TE-pass polarizer for silicon photonics," in *Optical Fiber Communication Conference*, paper JTh1A.27 (2013).

1. Introduction

Silicon photonics is attracting more and more attention as the performance of the devices such as modulator and photo-detector on this platform approaching the traditional counterparts [1]. On the same time, owing to high-index-contrast between silicon and dioxide, the size of devices is much reduced compared with traditional planar lightwave circuits on silica. The compact integration of transmitter and receiver on a single silicon chip is closing to reality.

The cost of high integration is also obvious: higher index-contrast corresponds to smaller mode size resulting in high coupling loss with single mode fiber. To bridge silicon waveguide and fiber, mode size converter [2–7], which can expand the mode size of the silicon waveguide, is used to reduce the coupling loss. Among all the methods, the inversely tapered spot size converter (SSC) [2] is widely applied due to the simple structure and acceptable coupling loss. But this taper structure may introduce problem in some situations, which is seldom mentioned in previous literature. Figure 1(a) shows the measured transmission spectrum of a straight waveguide with SSC of IME's standard design for MPW platform [1] at the two ends. The curves are normalized with the light source as shown in Fig. 1(b). A polarization controller is used to control the polarization state of the input light, and an in-line polarizer is used to distinguish the polarization components in the output light. The spectrum of the light source was measured by directly connecting the PC controller and inline polarizer. TE(TM)-TM(TE) denotes the measured TM(TE) component with TE(TM)-polarized input light. There are periodic fluctuations in both the TE and TM components regardless the polarization state of the input light in the spectrum, also the polarization extinction ratio (PER) is much deteriorated compared with that of the source. However, the fluctuation becomes not so clear if the total output power is measured which can be simply realized by removing the in-line polarizer. Obviously, just a straight waveguide cannot generate the fluctuations. It is not due to Fabry-Perot effect either, which should have much short period considering the length of the waveguide. We find if there is polarization rotation effect in the SSC, the measured phenomena can be explained perfectly. Following is our analysis.

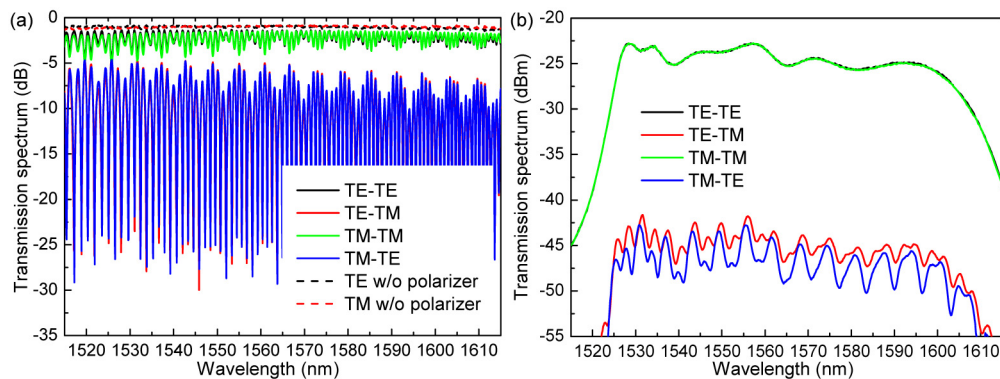


Fig. 1. (a) The normalized transmission spectrum of a straight waveguide with SSC at the both ends. (b) The spectrum of the input light.

2. Analysis

2.1. Origin of the polarization rotation effect in SSC

The width of the tip in the SSC is normally smaller than the height. In IME's devices library of the MPW platform, the width and height of the tip are 180 nm and 220 nm. However, the width of the waveguide is between 400~600nm in most of the application. Therefore, there is one position in the taper where the width equals to the height. For an ideal square waveguide with same material as up- and down-cladding layers, the effective index of the TE_0 and TM_0 modes will be equal in this position as shown in Fig. 2(a). There will not be coupling between the TE_0 and TM_0 modes due to the orthogonality of the modes. However, there are two factors, which may break the orthogonality and generate coupling between the two modes. Firstly, the up-cladding of the silicon waveguide is normally SiO_2 deposited with PECVD, while the down-cladding is thermal oxide in SOI wafer, there will be little difference about 0.02~0.03 in the refractive index of the two materials. Secondly, the sidewall of the waveguide is not ideally vertical, and the two sidewalls of the waveguide may be not totally same due to the lithography limit and transferred to waveguide in the etching as shown in Fig. 2(b), which means the waveguide is asymmetric in the cross section. The asymmetry will introduce perturbation to the modes and the two orthogonal TE_0 and TM_0 modes will be degenerated around designed square position and there should be coupling between the two modes, which means polarization rotation.

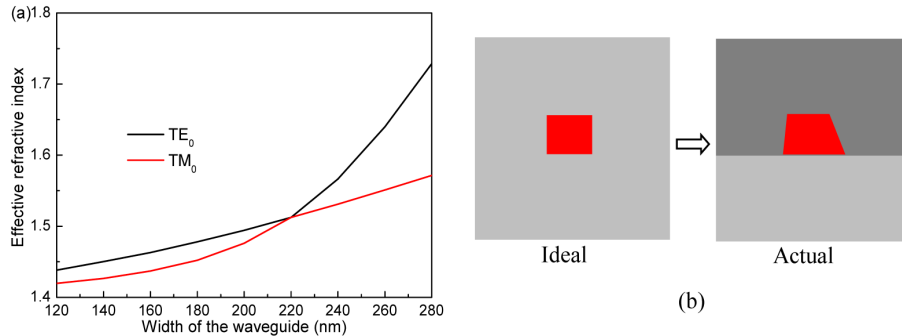


Fig. 2. (a) Effective indices of the first two modes as a function of the waveguide width in the channel waveguide with height of 220 nm. (b) The schematic cross-section of the ideal and actual Si waveguide.

We calculated the rotation coefficient of the asymmetrical waveguide with the method described in [8]. One of the sidewall is assumed to be vertical and another with an angle. The dependence of the rotation coefficient on the angle of the sidewall and width of the waveguide is simulated as shown in Fig. 3. Waveguide with width of 240 nm, not 220nm, has the most obvious rotation effect, it can realize complete rotation with proper angle. Since the SSC is a taper structure, it is difficult to estimate the rotation coefficient of the whole structure. But if the tip width is smaller than 240nm, the rotation effect is ignorable.

In general, this rotation effect may be not obvious, but it can still affect the polarization-dependence applications, in some specific situation, it is even fatal.

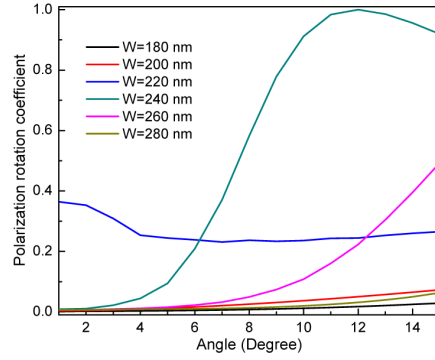


Fig. 3. Calculated polarization rotation coefficient as a function of the angel of the sidewall and the width of the waveguide.

2. 2. Light transmission in straight waveguide with SSCs

After explaining the principle of the polarization rotation effect of the SSC, following is the analysis of the light transmission in the straight waveguide with SSCs. We used the coupling matrix method to analyze the polarization rotation effect of the SSC and the transmission matrix method for the propagation of the light in the straight waveguide. Figure 4 shows the schematics of the TE-polarized input light transmission in the straight waveguide. The following deduction is also based on TE-polarized input light, which is applicable to TM-polarized input light.

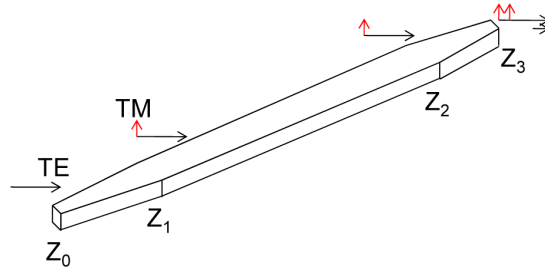


Fig. 4. Schematics of the TE-polarized input light transmission in the straight waveguide with SSC at the both ends.

TE-polarized input light can be expressed with vector:

$$E_{in} = E(z_0) = \begin{bmatrix} E_0 \\ 0 \end{bmatrix}, \quad (1)$$

E_0 is the normalized electrical field obeying the relation of $P_0 = E_0^2$, where P_0 is the power of input light. The polarization effect of the SSC can be express with the following matrix:

$$\begin{bmatrix} \tau & i\kappa \\ i\kappa & \tau \end{bmatrix}, \quad (2)$$

where τ is the transmission coefficient, κ is the rotation coefficient, both parameters are wavelength dependence and they should obey the relation:

$$\tau(\lambda)^2 + \kappa(\lambda)^2 = 1. \quad (3)$$

Considering the coupling loss of the SSC, the optical field after SSC is:

$$E(z_1) = \begin{bmatrix} \tau & i\kappa \\ i\kappa & \tau \end{bmatrix} \begin{bmatrix} e^{-\frac{\alpha_{CTE}}{2}} & 0 \\ 0 & e^{-\frac{\alpha_{CTM}}{2}} \end{bmatrix} \begin{bmatrix} E_0 \\ 0 \end{bmatrix}, \quad (4)$$

where $\alpha_{CTE/TM}$ is the coupling loss of the TE and TM mode in the SSC. After propagation in the straight waveguide, the optical field is

$$E(z_2) = \begin{bmatrix} e^{i\beta_{TE}L - \frac{\alpha_{TE}}{2}L} & 0 \\ 0 & e^{i\beta_{TM}L - \frac{\alpha_{TM}}{2}L} \end{bmatrix} \begin{bmatrix} \tau & i\kappa \\ i\kappa & \tau \end{bmatrix} \begin{bmatrix} e^{-\frac{\alpha_{CTE}}{2}} & 0 \\ 0 & e^{-\frac{\alpha_{CTM}}{2}} \end{bmatrix} \begin{bmatrix} E_0 \\ 0 \end{bmatrix}, \quad (5)$$

where $\alpha_{TE/TM}$ and $\beta_{TE/TM}$ are separately the propagation loss and propagation constant of the TE and TM mode in the waveguide, L is the length of the straight waveguide. After passing through the SSC in the output port, the optical field is:

$$E(z_3) = \begin{bmatrix} e^{-\frac{\alpha_{CTE}}{2}} & 0 \\ 0 & e^{-\frac{\alpha_{CTM}}{2}} \end{bmatrix} \begin{bmatrix} \tau & i\kappa \\ i\kappa & \tau \end{bmatrix} \begin{bmatrix} e^{i\beta_{TE}L - \frac{\alpha_{TE}}{2}L} & 0 \\ 0 & e^{i\beta_{TM}L - \frac{\alpha_{TM}}{2}L} \end{bmatrix} \begin{bmatrix} \tau & i\kappa \\ i\kappa & \tau \end{bmatrix} \begin{bmatrix} e^{-\frac{\alpha_{CTE}}{2}} & 0 \\ 0 & e^{-\frac{\alpha_{CTM}}{2}} \end{bmatrix} \begin{bmatrix} E_0 \\ 0 \end{bmatrix}. \quad (6)$$

After calculation, the field in the output port is:

$$E(z_3) = \begin{bmatrix} (\tau^2 e^{i\beta_{TE}L - \frac{\alpha_{TE}}{2}L} - \kappa^2 e^{i\beta_{TM}L - \frac{\alpha_{TM}}{2}L}) e^{-\alpha_{CTE}} E_0 \\ i\kappa\tau \left(e^{i\beta_{TE}L - \frac{\alpha_{TE}}{2}L} + e^{i\beta_{TM}L - \frac{\alpha_{TM}}{2}L} \right) e^{-\frac{\alpha_{TM} + \alpha_{TE}}{2}} E_0 \end{bmatrix}, \quad (7)$$

and the power is:

$$P(z_3) = \begin{bmatrix} P_0 e^{-2\alpha_{CTE}} \left(\tau^4 e^{-2\alpha_{TE}L} + \kappa^4 e^{-2\alpha_{TM}L} - 2\tau^2\kappa^2 e^{-(\alpha_{TE} + \alpha_{TM})L} \cos \Delta\theta \right) \\ P_0 e^{-(\alpha_{CTM} + \alpha_{CTE})} 2\kappa^2\tau^2 e^{-(\alpha_{TE} + \alpha_{TM})L} (1 + \cos \Delta\theta) \end{bmatrix}, \quad (8)$$

where $\Delta\theta$ is the phase difference between the TE and TM mode after propagation in the straight waveguide, it is further expressed as:

$$\Delta\theta = \theta_1 - \theta_2 = (\beta_{TE} - \beta_{TM})L = \frac{2\pi(n_{effTE} - n_{effTM})}{\lambda}, \quad (9)$$

where n_{effTE} and n_{effTM} are the effective indices of the TE and TM mode. For TM-polarized input light, the output power is:

$$P(z_3) = \begin{bmatrix} P_0 e^{-(\alpha_{CTM} + \alpha_{CTE})} 2\kappa^2\tau^2 e^{-(\alpha_{TE} + \alpha_{TM})L} (1 + \cos \Delta\theta) \\ P_0 e^{-2\alpha_{CTM}} \left(\tau^4 e^{-2\alpha_{TM}L} + \kappa^4 e^{-2\alpha_{TE}L} - 2\tau^2\kappa^2 e^{-(\alpha_{TE} + \alpha_{TM})L} \cos \Delta\theta \right) \end{bmatrix}. \quad (10)$$

Aforementioned is the mathematics deduction of the light transmission in the waveguide. In physics scenario, the final field is the interference of two optical fields: through the input SSC, partial of the input light is converted to TM(TE) component from TE(TM) component. After propagation through the straight waveguide, the TE and TM modes have different phase due to different propagation constant of the modes. After passing the output SSC, partial of the TE and TM components will be transferred to each other. Then the rotated TE/TM components will interfere with the remaining TE/TM components due to the phase difference.

3. Comparison between the analysis and measurement results

Figure 5 is the transmission spectrum of a straight waveguide with width of 500 nm and length of $\sim 2600 \mu\text{m}$. There are two fundamental modes TE_0 and TM_0 in the waveguide. The SSC has a tip width of 180nm and length of $200 \mu\text{m}$. According to the deduction results, there should be several properties in the transmission spectrum:

1. There is π phase difference between the TE and TM components in the output.

The coincidence of the constructive and destructive wavelength in the curves TE(TM)-TE(TM) and TE(TM)-TM(TE) in Fig. 5 clearly show the π phase difference between them.

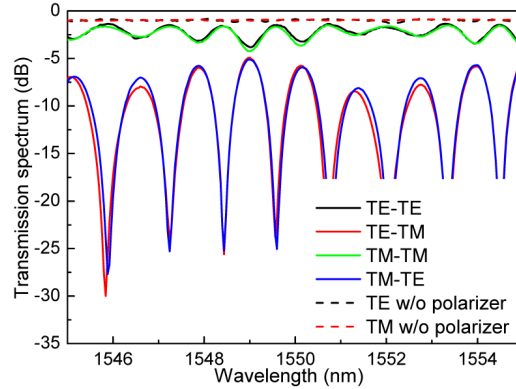


Fig. 5. Zoomed-in image of the transmission spectrum in Fig. 1(a).

2. The fluctuation amplitude of the TE(TM)-TM(TE) component should be much higher than that of the TE(TM)-TE(TM) since the rotation effect of the SSC is weak in most situation. According to the Eqs. (8) and (9), the TE(TM)-TM(TE) should have infinite fluctuation amplitude. This phenomenon is also clearly shown in Fig. 5.

3. The period of the fluctuation can be deduced from Eq. (9):

$$\Delta\lambda = \frac{\lambda^2}{L(n_{\text{effTE}}(\lambda) - n_{\text{effTM}}(\lambda))}. \quad (11)$$

It is related to the efficient index difference of TE and TM modes and the length of the straight waveguide. Meanwhile, the period should be same for both TE and TM-polarized input light, which is obvious in Fig. 5. As a contrast, the period due to Fabry-Perot effect is related to the effective index of the modes. Therefore, the TE and TM modes should have different period. According to Eq. (11) and the simulated effective indices of the channel waveguide as shown in Fig. 6, this sample will generate interference with period of 1.23 nm. The measured period around 1550 nm is about 1.2 nm as shown in Fig. 5, which matches very well with the calculation result. While the period due to the Fabry-Perot effect in the same waveguide is just about 0.1 nm, which is just one tenth of the measurement result.

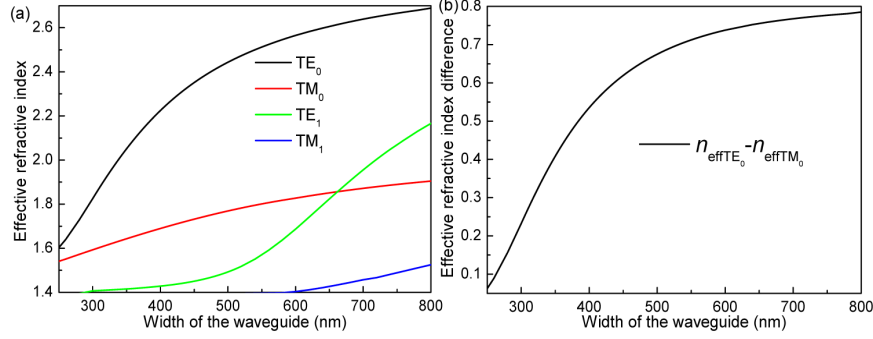


Fig. 6. (a) Effective indices of the first four modes in the channel waveguide as a function of the waveguide width. (b) The effective index difference between the TE₀ and TM₀ modes as a function of the waveguide width.

4. If the coupling loss for TE and TM modes is same, the total output power will be:

$$P_{\text{total}}(z_3) = P_0 e^{-2\alpha_c} \left(\tau^2 e^{-\alpha_{TE}L} + \kappa^2 e^{-\alpha_{TM}L} \right)^2, \quad (12)$$

where α_c is the coupling loss of the two polarization modes. From Eq. (12), we can conclude that the interference in the output spectrum will disappear. To verify this conclusion, we removed the in-line polarizer at the output end and did not distinguish the TE and TM components in the output light. The fluctuation disappeared in the measured spectrum as the dashed curves shown in Fig. 8. Actually, the later setting is more common in test [1]. We usually control the polarization state of the input light and regard that the output light has same polarization state with the input light. This explains why we haven't observed the interference spectrum in most of the test.

5. If we further assume TE and TM modes have same propagation loss in waveguide, Eq. (8) can be simplified to

$$P(z_3) = \begin{bmatrix} P_0 e^{-2\alpha_c} e^{-2\alpha L} \left(\tau^4 + \kappa^4 - 2\tau^2 \kappa^2 \cos \Delta\theta \right) \\ P_0 e^{-2\alpha_c} 2\kappa^2 \tau^2 e^{-2\alpha L} (1 + \cos \Delta\theta) \end{bmatrix}, \quad (13)$$

where α is the propagation loss of the two polarization modes. The ratio of maximum of TE and TM modes can be expressed as

$$\frac{P(Z_3)_{TE \max}}{P(Z_3)_{TM \max}} = \frac{(\tau^2 + \kappa^2)^2}{4\kappa^2 \tau^2}. \quad (14)$$

Combined with Eq. (3), the transmission coefficient τ and rotation coefficient κ can be calculated with the measured spectrum. Figure 7 shows the calculated coefficients of two samples. The structure of the two samples will be explained in following paragraph. It is clear that these coefficients are wavelength-dependent and periodic. The envelope of the interference spectrum shown in Fig. 1(a) is the reflection of this phenomenon.

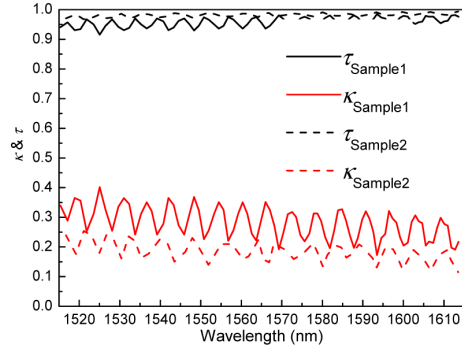


Fig. 7. The calculated transmission coefficient and rotation coefficient of the SSC. Solid and dashed lines are for sample 1 and sample 2 separately.

For further understanding the rotation effect of the SSC, we compared four different samples: Sample 1 is the straight waveguide we used in the previous analysis, which goes through triple Si etching in the fabrication process [9]; Sample 2 has exactly same design with Sample 1 but just goes through twice Si etching [1]; Sample 3 has same design with Sample 1 except for with width of 400 nm and also goes through twice Si etching as sample 2; Sample 4 is a channel waveguide with multiple bends of radius 5 μ m, which can work as TE-pass polarizer [10], it also has width of 500 nm and goes through triple Si etching. Same SSC structure is used in all the samples. Figure 8 shows the transmission spectrum of the four samples under same test condition. The insets in Figs. 8(a)–8(c) are the zoomed-in spectrum around 1550 nm to clearly display the period of the interference.

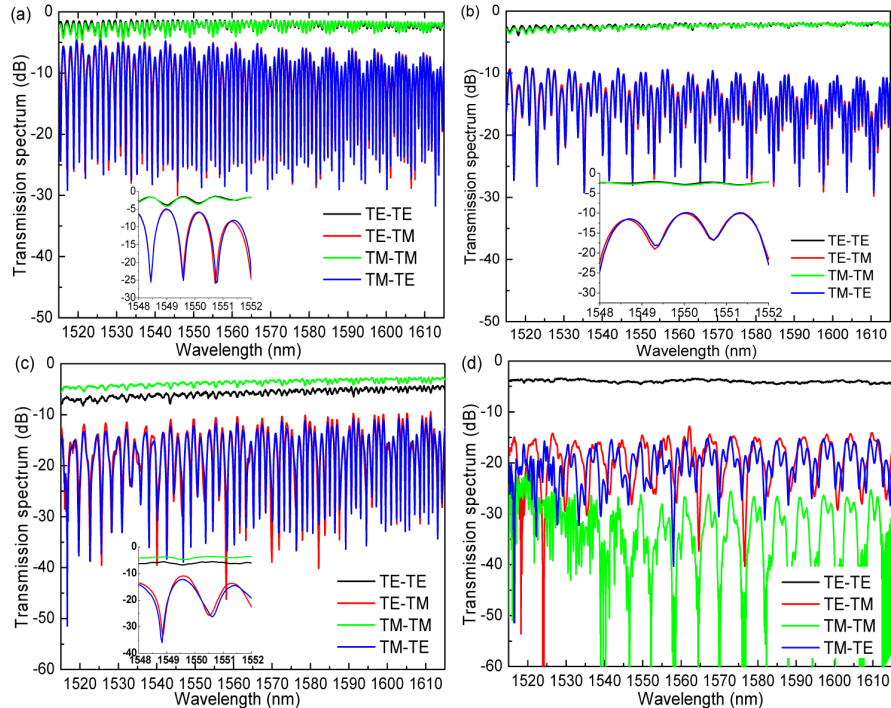


Fig. 8. Transmission spectrum of the four different samples.

Comparing Figs. 8(a) and 8(b), Sample 2 has smaller interference amplitude, which means the SSC in Sample 2 has weaker rotation effect. This is also confirmed by the calculated

transmission and rotation coefficients in Fig. 7. The reason for that is the triple Si etching in the fabrication makes the waveguide more asymmetric than the that with twice Si etching, while the asymmetry makes the rotation effect obvious. Figure 9 shows the cross-sectional TEM images of the two samples in a position of the SSC. Both waveguides are not ideally square and the sidewalls on both sides of the waveguides are also not symmetric, which introduces perturbation to the waveguide and degenerate the orthogonal TE_0 and TM_0 modes. Compared to sample 2, sample 1 has more asymmetrical cross-section therefore with more obvious polarization rotation effect.

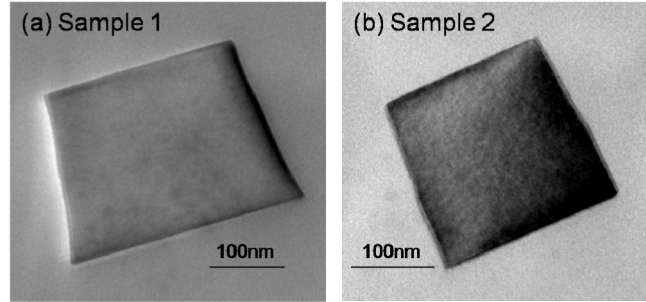


Fig. 9. TEM images of the cross-section in a position of SSC. (a) Sample 1; (b) Sample 2.

The insets in Figs. 8(a)–8(c) are the zoomed-in spectrum around 1550 nm. The three samples have periods of 1.2 nm, 1.31 nm and 1.72 nm separately. Since narrower waveguide has smaller effective index difference according to the results in Fig. 6, the phenomenon is reasonable. Sample 1 and 2 have same design width, but they were fabricated on different wafers and went through different etching process, the actual width of the waveguide cannot be totally same, that explains the little difference in the period of the two samples.

In sample 4, the multiple small bends can block the TM_0 mode in the waveguide. Combined with the analysis in section 2.2, the four components TE-TE, TE-TM, TM-TM and TM-TE in the output light are proportional to τ^2 , $\kappa\tau$, κ^2 , and $\kappa\tau$ separately. The interference cannot be set up again in the output. While the fluctuation in Fig. 8(d) is due to the wavelength dependence of κ and τ as shown in Fig. 7, which can be simply deduced from the period of the fluctuation. Sample 4 provides a method to remove the influence of rotation effect of the SSC in the input port.

4. Discussion

For expanding the communication bandwidth, dual-polarization based application has become more common [11,12]. However, the SSC, as the interface of the chip to optical fiber network, may introduce crosstalk between the two polarization states due to the polarization rotation effect. According to Eq. (13), the maximal crosstalk for TE-polarized input light can be expressed as

$$Crosstalk_{\max} = \frac{P(Z_3)_{TE \min}}{P(Z_3)_{TM \max}} = \frac{(\tau^2 - \kappa^2)^2}{4\kappa^2\tau^2}. \quad (15)$$

For a dual-polarization quadrature phase-shift-keying (DP-QPSK) signal, it requires 12.5 dB optical signal-to-noise ratio (OSNR) to obtain BER of 10^{-3} at 15.75Gbaud/s [13]. However, the crosstalk is as high as 12.5 dB even for $\tau = 0.9932$, which means a very tiny rotation effect in the SSC can generate non-neglectable crosstalk in the polarization multiplexing system. Fortunately, this crosstalk is the intrinsic property of the structure and measurable, it can be compensated with proper algorithm in the data processing of the system [14].

According to all the analysis, the asymmetry of the waveguide in vertical direction is the main cause of the polarization rotation effect of the SSC, reducing the etching times of the waveguide is an effective method to reduce the asymmetry. Adding a polarizer [15] after the SSC can also release the impact especially the interference effect.

There are other structures that may generate detrimental polarization rotation in the waveguide. If a taper structure covers the crossing point of the curves TE_1 and TM_0 in Fig. 6, there may be also polarization rotation from TM_0 to TE_1 and crosstalk between the two polarization states.

5. Conclusion

The polarization rotation effect in the SSC is normally weak but it is still possible to generate detrimental impact to the polarization-dependent applications. Several methods are suggested to release the effect but it is difficult to remove it from the root. We will keep studying on this topic.

Acknowledgment

This work was supported by A*STAR (Agency for Science, Technology and Research) – MINDEF Science and Technology Joint Funding Program under Grant No.1223310076 and the Science and Engineering Research Council of A*STAR under Grant No. 1323300001.